Metallomics

Accepted Manuscript

This article can be cited before page numbers have been issued, to do this please use: M. C. Ruiz, J. Kljun, I. Turel, A. L. Di Virgilio and I. Leon, *Metallomics*, 2019, DOI: 10.1039/C8MT00369F.

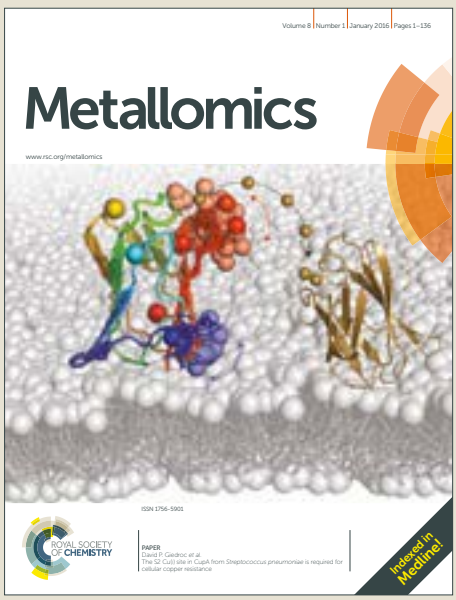

ROYAL SOCIETY OF CHEMISTRY

rsc.li/metallomics

View Article Online
DOI: 10.1039/C8MT00369F

We have developed a novel family of antitumor organoruthenium 8-hydroxyquinolinato complexes, that used different substituted 8-hydroxyquinoline derivatives as ligands One of these compounds (1) was demonstrated to exert stronger anticancer and antimetastatic effects than cisplatin on 2D and 3D multicellular spheroids derived from human lung cancer cells. These findings show that compound 1 is an interesting candidate for potential antitumor uses and provide new insight into the design and development of ruthenium compounds as potential anticancer agents.

.

Comparative antitumor studies of organoruthenium complexes with 8-hydroxyquinolines on 2D and 3D cell models of bone, lung and breast cancer

Maria C. Ruiz [1], Jakob Kljun[2], Iztok Turel [2], Ana L. Di Virgilio [1] *, Ignacio E. León [1] *

[1] Inorganic Chemistry Center (CEQUINOR, CONICET), Exact School Sciences, National University of La Plata, Bv 120 1465, 1900 La Plata, Argentina

[2] Faculty of Chemistry and Chemical Technology, University of Ljubljana, Večna pot 113, 1000 Ljubljana, Slovenia.

* Corresponding author: ileon@biol.unlp.edu.ar , aldivirgilio@biol.unlp.edu.ar

Abstract

The purpose of this work was to screen the antitumor actions of two metal organoruthenium–8-hydroxyquinolinato (Ru-hq) complexes to find a potential novel agent for bone, lung and breast chemotherapies. We showed that ruthenium compounds (**1** and **2**) impaired the cell viability on human bone (MG-63), lung (A549) and breast (MCF7) cancer cells with greater selectivity and specificity than cisplatin. Besides, complexes **1** and **2** decreased proliferation, migration and invasion on cell monolayers at lower concentrations (2.5-10 μM). In addition, both compounds induced genotoxicity revealed by the Micronucleus test, which conveys into G_2/M cell cycle arrest and undergoes the tumor cells to apoptosis.

On the other hand, in multicellular 3D models (multicellular spheroids; MCS), **1** and **2** overcame CDDP presenting lower IC_{50} values only in MCS of lung origin. Moreover, **1** outperformed **2** in MCS of bone and breast origin.

Finally, our findings revealed that both compounds inhibited the cell invasion of multicellular spheroids, showing that complex **1** exhibited the most important antimetastatic action.

Taken together, these results indicate that compound **1** is an interesting candidate to be tested on *in vivo* models as a novel strategy for anticancer therapy.

Introduction

Cancer is one of the leading causes of death worldwide [1]. Uncontrollable dividing and spreading cells are the main feature of this disease. Unfortunately, despite the fact that in

recent years chemotherapy has been successful in increasing the 5-year survival rate to over 80% in certain types of cancers (Hodgkin lymphoma, testicular, etc) there has not been the same accomplishment for other more aggressive tumors, which still have extremely low survival rates [2]. Therefore, new strategies for the treatments including novel chemotherapeutic drugs are highly required to improve prognosis.

Metal-based compounds are a class of anticancer drugs largely used in the treatment of many kind of tumors, such as lung, prostate, colon, and breast cancers [3,4].

Since the discovery of cisplatin (CDDP), several platinum-based complexes are extensively used in the clinical treatment of particularly testicular and ovarian cancers [5]. However, drug resistance to cisplatin developed by cancer cells and several side effects of platinum compounds have led to a novel research line focusing on the potential of ruthenium chemotherapeutics [6].

In this sense, many ruthenium compounds show promising anticancer activity, especially the leading complex KP1019 that is currently undergoing clinical trials (Phase I and II) [7–9]. Besides, several ruthenium complexes show deleterious effects on tumor cells by modulating various cellular processes including migration, proliferation and cell differentiation [10,11].

One of the main strategies used in metallodrug design is the binding of metal fragments to known pharmacophores such as 8-hydroxyquinolines [12]. This group of ligands display antibacterial, antifungal, antiviral and anticancer activities and their action is often attributed to the interaction with metal ions which are relatively abundant in biological systems [13,14]. In addition, hydroxyquinolines have been used as ligands in the design of metal based drugs through the relevant physicochemical properties of their coordination compounds [15,16]. Recent studies show that coordination compounds of copper, platinum, vanadium and ruthenium present remarked anticancer activity toward bone, colon, leukemia, lung cells [16–21].

In this context, we have developed a novel family of antitumor organoruthenium and also platinum 8-hydroxyquinolinato complexes, that used different substituted 8-hydroxyquinoline derivatives as ligands [22,23]. In both studies we have found a very similar influence of the halogen-substitution pattern of 8-hydroxyquinolinato moiety on the anticancer activity- the introduction of the bromo substituents on positions 5 and 7 resulted in increased toxicity in three different cell lines. Based on these results, we aimed to explore the therapeutic potential of organoruthenium 8-hydroxyquinolinato complexes as antitumor agents. This study deals with the antitumor effects of two the most successful

previously selected[22] organoruthenium 8-hydroxyquinolinato complexes (**1** and **2**, Figure 1) on a normal cells (L929) and human cancer panel cell lines including bone (MG-63), lung (A549) and breast (MCF7 and MDA-MB-231). In particular, we focused our research on the action of both complexes on the cell viability, cell cycle arrest and apoptosis and the effects of ruthenium compounds over migration and invasion of tumor cells.

Finally, we have investigated the antiproliferative and antimetastatic actions of both compounds using 3D multicellular spheroids (MCS) derived from bone, lung and breast cell lines.

Results and discussion

Stability studies of complexes 1 and 2

The electronic absorption spectrum of complex **1** and **2** is determined in Dulbecco's modified Eagle's medium (DMEM).

In the electronic absorption spectrum of compound 1 (0.001 M in DMEM solution) one band was observed at 405 nm (e =4400 M^{-1} cm^{-1}). Upon monitoring this solution with time (0.25, 0.5, 1, and 24 h), no changes were observed in the UVvis signals, and the integrity of the complex in culture medium was intact within the time-frame of the biological experiments. Besides, in the electronic absorption spectrum of compound **2** (0.0001 M in DMEM solution) one band was observed at 276 nm (e = 50000 M^{-1} cm^{-1}) and upon monitoring this solution no changes were observed.

These results suggest that the compound **1** and **2** does not undergo oxidation and is stable over time.

Besides, we have carefully studied the stability of the parent Ru-clioquinol and the results showed that no changes were observed in the NMR signals, and the integrity of the complex in DMSO solution as well as the aqua species in 10% DMSO aqueous solution was intact within the time-frame of the biological experiments [24] . Moreover, the stability of the complex in the presence of phosphate buffers was monitored by UV-Vis spectroscopy and the spectra remain unchanged after 24 hours [24].

On the other hand, Kubanik and coworkers [25] performed stability studies of 5 Ru-hq complexes and they determined that the complexes are stable in dmso-d_6 and D_2O.

View Article Online
DOI: 10.1039/C8MT00369F

Effect of complexes 1 and 2 on cell viability and cell proliferation

Cytotoxicity studies, determined by the MTT assay [26], were carried out for both compounds with MG-63 (human osteosarcoma), A549 (lung adenocarcinoma), MCF7 (breast adenocarcinoma) cells. Clinical agent cisplatin was used for reference. The IC_{50} values with the three different cell lines are recorded in Table 1.

Table 1 shows that compound **2** exhibits better cytotoxic activity after 24 h of incubation on human tumor cells tested than compound **1** showing higher IC_{50} values for all the tumor cell lines. Moreover, both compounds are more active than CDDP in all the tested cell lines.

To understand the specific potential of compounds **1** and **2** and to address its selectivity for cancer cells, we investigated their effect on the cell viability of mouse derived fibroblast (L929 cells) and we compared their effects by calculating the selectivity index (SI).Table 1 shows that while 1 has great selectivity on MG-63 and MDA-MB-231, 2 has great selectivity on the four tumor cell lines tested.

Besides, in all tumor cell lines tested both compounds showed better selectivity performance than cisplatin. This great selectivity may be explained based on the mode of action of ruthenium complexes. The most accepted mechanism of action is the redox balance disruption, which leads to cell cycle arrest on G2/M, DNA synthesis blockage and finally apoptosis induced mitochondrial pathway [27]. On the other hand, cancer cells undergo an increased steady-state ROS condition compared to normal cells, which may represent an Achilles' heel of cancer cells that may be exploited therapeutically, as a small increase in ROS levels may overcome the toxic threshold, leading to apoptotic cell death [28].

On the other hand, the clonogenic assay was performed to evaluate the effect of the complexes on the cellular reproductive potential. Figure 2 shows a clear reduction of cell proliferation which agreed with the cell viability assay on MG-63, A549 and MCF7 cells. In addition, both compounds affected the colony formation in a dose-dependent manner (2.5-10 μM $^{\#}p<0.01$). Again, **2** demonstrated greater inhibition effect than **1** ($^{*}p<0.01$).

In this order**,** several ruthenium compounds showed cytotoxic activity in the low micromolar (μM) range in various cell lines but many of them lack selectivity.[29]

Only a few Ru(II)-based complexes presented selectivity to cancer cells when evaluated by clonogenic assay in Caco-2 monolayers [30] or against two human cancer cell lines

(HeLa and A549 cancer cell lines) in comparison to normal cell line BEAS-2B (Human bronchial epithelial cells) by the MTT assay [31].

Effect of complexes 1 and 2 on cell migration and invasion

Next, we evaluated the effect of **1** and **2** on cell migration (wound healing assay) and invasion (single cell lamellipodia assay) on bone (MG-63), lung (A549) and breast cancer (MCF7) cells. Our wound healing results (Figure 3A-C) showed that both ruthenium compounds inhibited the cell migration in the tumor cell lines studied. Both compounds inhibited bone and breast tumor cell migration to almost half the untreated cells. Nevertheless, on A549 cells only compound **2** inhibited the cell migration at 2.5 μM in the range of concentrations tested (2.5 and 5 μM).

On the other hand, Figure 4 shows that **2** outperformed **1** on cell invasion of MG-63, A549 and MCF7 cells. As it can be seen from Figure 4, compound **2** has much stronger antimetastatic effects than **1** in the range of 2.5-25 μM and demonstrates to be more specific according to the following order: MCF7>MG-63>A549.

These results on cell migration and invasion along with the effect on clonogenic capacity and the IC_{50} values point out to complex **2** as the best candidate as antitumor agent, and bone or breast tumor cells to be more susceptible in comparison to lung carcinoma cells.

Effect of complexes 1 and 2 on CT DNA interaction

The affinity of complexes **1** and **2** for CT DNA was evaluated using UV spectroscopy titrations, as an initial approach to obtain data concerning their possible targets and provide information about the mechanism.

Figure SM1 showed that both complexes increasing the emission observed at 268 nm (complex **1**) and 275 nm (complex **2**) suggesting the presence of hyperchromic effect. The intrinsic binding constant Kb was determined by using Wolfe-Shimer equation., Kb for complex **1** is $7.43 \times 10^{4}\ M^{-1}$ and for complex **2** is $9.61 \times 10^{4}\ M^{-1}$. These values, recorded in the first 10 minutes of reaction, seemed to indicate that the reactivity of the complexes **1** and **2** could be understood as having a good affinity for CT DNA in a non-covalent binding mode of action. The observed hyperchromic phenomenon reflects structural and conformational changes in DNA induced by both complexes suggesting that DNA may be at least at partly one of the main molecular targets of these kinds of

complexes. Nevertheless, the reactivity observed is quite different to cisplatin, which is as a covalent binder reported to produce two effects: hyperchromic and bathochromic [32]. Besides, different platinum and palladium complexes shows similar values of K constants [33]. Thus, the results suggest that DNA could be a molecular target of both complexes.

Genotoxic effects of complexes 1 and 2

The genotoxic effect of **1** and **2** (Figure 5) was studied through the increase of the micronucleus frequency, which are cytoplasmic bodies having a portion of an acentric chromosome or the whole chromosome that was not carried during anaphase [34].

In MG-63 cells, only compound **2** after incubation with 2.5 μM increased the micronucleus fractions ($^{\#}p < 0.01$). In A549-treated cells, **1** induced micronuclei formation from 2.5 μM, while **2** showed a pronounced response from 1 μM. This effect tripled the level of the control group ($^{\#}p < 0.01$). At 1 μM, complex **2** showed a stronger genotoxicity effect than complex **1** ($^{*}p < 0.01$).In addition, in MCF7 cell line, both complexes increased the micronucleus fraction from 5 μM ($^{\#}p < 0.01$).

Altogether, these results show that both compounds induced genotoxicity in three tumor cell lines at lower concentrations suggesting that DNA may be a molecular target involved in the antitumor actions. It was reported before that numerous ruthenium complexes may also exert antiproliferative effects via interactions with DNA, inducing cleavage, break, and intercalation of DNA strands [35–37].

Moreover, even though ruthenium(II) based compounds presented anti-proliferative activity against HepG2 and MDA-MB-231 tumor cells and could bind to DNA through electrostatic interactions, no mutagenicity was detected when they were evaluated by cytokinesis-blocked micronucleus assay and Ames test in the presence and absence of S9 metabolic activation from rat liver [38] Likewise, *in vivo* studies showed that ruthenium-based anticancer agents did not cause genetic toxicity, presenting a lack of micronuclei formation and low DNA damage induction in the cells from Swiss mice in spite of the promising results as anticancer agents [39].

Cell cycle analysis and apoptosis

One hot-topic emerging in drug discovery is to develop agents that inhibit cell cycle checkpoints that are responsible for the control of cell cycle phase progression. Cell cycle

arrest as a function of the concentration of both compounds on MG-63, A549, MCF7 cell lines was analyzed by flow cytometry. Figure 6 and SM2 show that the three types of tumor cells were arrested at S and G_2/M phase after incubation with compounds **1** and **2** ($p<0.01$). In this order, compound **1** induced MG-63 cell cycle arrest on S phase while compound **2** increased the fractions of MG-63 arrested cells on G_2/M phase at the lowest concentration and in S phase at the highest. Both complexes induced a A549 cell cycle arrest in S phase at the lowest concentration studied, but when the concentration was increased the cells are arrested in G_2/M and S phases in comparison to the untreated cells. In MCF7 cells, compound **1** and **2** increased the S phase fraction-arrested cells in a concentration manner response (5-15 μM).

Apoptosis is a physiological process of cell death enhanced in the presence of injurious drugs [40], characterized by morphological and biochemical changes. One of the first modification is the externalization of phosphatidylserine at the outer plasma membrane leaflet. Annexin V–FITC is a fluorescent dye with high affinity for phosphatidylserine allowing its determination by fluorescence assays. Table 2 shows that both compounds increased the early (Annexin V positive) and late apoptotic (Annexin V positive /PI positive) cell fractions on MG-63 and MCF7 but did not observe proapoptotic effects on A549 cells. Moreover, the necrotic population (Annexin V negative /PI positive) also rose to the detriment of the living cells after treatment of both complexes in the tumor cell lines studied. MG-63 cell cultures showed an increase in the early and late apoptotic cellular fractions when were incubated with 5 μM of complex **1** or 10 μM of complex **2** ($p < 0.01$). MCF7 cells showed an increase of early and late apoptotic populations when exposed to both complexes; the induction of complex **2** being more pronounced.Our results demonstrate that both complexes raised the proportion of cells arrested in phase S and apoptosis induction in the three tumor cell lines studied and these effects are among the main processes that mediate the anticancer effects of both ruthenium compounds. Arresting cell cycle and inducing apoptosis have also been reported as the main mechanism of cytotoxicity for several ruthenium-based complexes in different tumor cell lines [41].

It is worth mentioning that the increase of S phase-arrested cell fraction could be associated with the increased in MN frequency. It has been demonstrated that micronuclei can be induced by chemicals that are known to cause DNA replication stress and S phase arrest, that is, cells bearing intrinsic genomic instability [42]. This phenomenon occurs during DNA replication and could result in a stalled replication fork [43].

View Article Online
DOI: 10.1039/C8MT00369F

3D studies

Effect of compound 1 and 2 on spheroids cell viability

To determine and compare the anticancer properties of compound **1** and **2**, we evaluated their effects on cell viability in MG-63, A549 and MCF-7 multicellular spheroids using the resazurin reduction assay. It is used as an oxidation-reduction indicator in cell viability assays for both aerobic and anaerobic respiration [44].

Table 3 shows the IC_{50} values for complex **1** and **2** on three types of MCS. Both compounds exert cytotoxic effects of MCS affecting the shape and the volume of the spheroids. In this way, the complex **1** shows a higher anticancer activity than complex **2** in the three MCS models ($p < 0.01$). Moreover, complex **1** showed better anticancer activity than cisplatin on MCS derived from A549 cells.

These results are in contrast to the 2D cell viability results in which complex **2** shows stronger antitumor activity than complex **1** suggesting that several factors like the redox potential, hypoxic conditions, cell uptake, bioavailability are key to define the anticancer activity of antitumor drugs [45]. In this way, Schreiber-Brynzak *et al.* suggested that the antitumor and antiinvasive activity of metallodrugs are dependent on the cell culture model used. These authors proposed that the combined use of different cell models (2D and 3D) provides a reliable informative basis about the compound activity to assess and better predict the antitumor potential of novel metal-based drugs [45]. Detailed comparison of results obtained for all tested metallodrugs shows that the use of 3D model results in a totally new ranking of compounds about their cytotoxicity *in vitro*. It is also worth to note that the cytotoxicity of the gallium complex KP46 and the ruthenium derivate KP1339 was markedly higher in the 3D spheroid model than in monolayer showing IC_{50} values of 0.44 μM (2D) vs 133 μM (3D) and 133 μM (2D) vs 244 μM (3D), respectively [45].

It is well known that the three-dimensional cell culture models represents a solid tumor environment that frequently shows decreased drug sensitivity, an event called multicellular resistance (MCR) [46]. The crucial reasons for the development of MCR are cell cycle changes, in particular a low fraction of dividing cells, changes on drug penetration due to cell-cell interactions and cell-matrix connections [47,48]. Moreover, other important factor is hypoxia that may contribute to resistance by inducing changes in expression of apoptosis factors [49]. In this sense, Gosch *et al.* reported the key role of

hypoxic conditions on the cytotoxic activity of platinum compounds on 2D and 3D cell models [50]. Those compounds showed a significantly decreased cytotoxicity on spheroids compared to normoxic monolayer culture in human colon cancer cells. In this way, an oxaliplatin-based compound is up to 20 times and oxaliplatin even 13–64 times less active in 3D tumor spheroids than in the 2D cell monolayer cultures [50].

Invasion studies

With the aim to elucidate and determine the antimetastatic effects of compound **1** and **2**, we evaluate their actions on cell invasion in MG-63, A549 and MCF7 multicellular spheroids visualizing the invasion on a collagen substrate. Figure 7 and SM3 show that complexes **1** and **2** inhibited cell invasion capacity of MG-63 (A), A549 (B) and MCF7 (C) multicellular spheroids in a concentration- manner response from 50 to 200 μM ($^{\#}p < 0.01$). Besides, as it can be seen from figures 7B and C, at 50 and 100 μM compound **1** has a stronger antimetastatic activity than compound **2** on lung and breast spheroids ($^{*}p < 0.01$). In addition, the antimetastatic effects of Ru compounds are in accordance with the 3D cell viability results in which the effects of compound **1** are higher than those of compound **2**.

It is well known that cells grown in spheroids produce increased amounts of adhesion molecules [51]. Therefore, the differences on anti-invasive activity of compound **1** and **2** on 2D and 3D invasion models could be explained based on changes in expression levels of adhesion molecules between MCS (3D) and monolayer culture (2D) [51].

Conclusion

The exhaustive characterization of the anticancer activity of two organoruthenium complexes with 8-hydroxyquinolines was performed in the frame of a multidisciplinary research project devoted to the design and development of ruthenium compounds with potential antitumor properties. In this sense, both tested compounds caused cyto- and genotoxicity in a concentration dependent manner on bone, lung and breast cancer cell lines. An important pharmacological fact is that both compounds showed high selectivity for tumor cells and were less active against normal phenotype cells such as normal L929 fibroblasts. In addition, complex **1** and **2** inhibited migration and invasion of bone, lung and breast cancer cells. On the other hand, complex **1** showed higher anticancer activity

than complex **2** on multicellular spheroids model which emphasizes the importance of cell uptake, hypoxia and drug bioavailability on antitumor activity. Likewise, compound **1** displayed higher deleterious effect than cisplatin on MCS derived from A549 cells. A stronger antimetastatic activity was also demonstrated by 1 on 3D collagen invasion assay.

Our findings indicate that compound **1** is an interesting candidate for potential antitumor uses and provide new insight into the design and development of ruthenium compounds as potential anticancer agents.

Experimental section

Synthesis and characterization of organoruthenium compounds

Complexes **1** and **2** were synthesized according to the previously reported results [22].

The identification of the complex was done by ^{1}H NMR, FTIR, UV-VIS and elemental analyses [22].

Preparation of Ru complexes solutions

Fresh stock solutions of both complexes (20 mM) were prepared in DMSO and diluted according to the concentrations indicated in the legends of the figures.

Precautions should be taken with the maximum concentration of DMSO in the well plate. We used 0.5 % as the maximum DMSO concentration to avoid toxic effects of this solvent on the cells.

Stability of the complex in solution

To test the stability of the compounds, we analyzed the UV-visible spectra of different solutions of the complex. 20 mM solutions of complex in DMSO and 0.1 mM of complex in medium DMEM (pH = 7.4) were prepared. The electronic spectra were recorded at times ranging from 0 to 24 h at 37 °C. The rate of decomposition of the complex was spectrophotometrically measured.

Cell line and growth conditions

Human osteosarcoma cell line (MG-63), human lung cancer cell line (A549), breast cancer cell line (MCF-7 and MDA-MB-231) and L929 (fibroblast, *Mus musculus*, mouse) were grown in Dulbecco's modified Eagle's medium (DMEM) containing 10% fetal bovine serum (FBS), 100 IU/mL penicillin and 100 µg/mL streptomycin at 37 °C in 5% CO_2 atmosphere. All cancer cell lines were grown in a 75 cm^2 flask until they reach 70–80% of confluence. Then, the cells were subcultured using TrypLE TM. For experiments, cells were grown in multi-well plates. Dulbecco's modified Eagle's médium (DMEM) and TrypLE TM were purchased from Gibco (Gaithersburg, MD, USA), and fetal bovine serum (FBS) was purchased from Internegocios (Argentina). After 24 h the monolayers were washed with DMEM and were incubated under different conditions according to the experiments. Tissue culture materials were purchased from Corning (Princeton, NJ, USA).

Cell viability: 3-(4,5-Dimethylthiazol-2-yl)-2,5-diphenyltetrazolium bromide assay

The 3-(4,5-dimethylthiazol-2-yl)-2,5-diphenyltetrazolium bromide (MTT) assay was performed according to Mosmann [26]. Briefly, cells were seeded in a 96-well dish, allowed to attach for 24 h, and treated with different concentrations of ruthenium complexes at 37º C for 24 h. Afterward, the medium was changed and the cells were incubated with 0.5 mg/mL MTT under normal culture conditions for 3 h. Cell viability was marked by the conversion of the tetrazolium salt MTT to a colored formazan by mitochondrial dehydrogenases. Color development was measured spectrophotometrically with a microplate reader (multiplate reader multiskan FC, thermo scientific) at 570 nm after cell lysis in DMSO (100 µL per well). Cell viability was plotted as the percentage of the control value.

Clonogenic assay

Cells were seeded in a 24 well plates, after attachment of the cells to the dishes, they were treated with either Ru complexes at a range of 2.5 to 10 µM. After 24 hours, the cells were washed with PBS and 2 ml of complete DMEM were add. The plates were incubated for 10 days at 37ºC and 5% CO_2. After this time, medium was removed, and cells were rinsed with PBS. Cells were stained with a mixture of 6% of glutaraldehyde and 0.5% of

crystal violet for 30 minutes at room temperature. Then, the plates were washed with distilled water and dried. After, we proceed to count the colonies.

The plating efficiency (PE) is the ratio of the number of colonies to the number of cells seeded whilst the number of colonies that survive after treatment, expressed in terms of PE, is called the surviving fraction (SF).

Wound healing assay

Cells were grown in a 12 well cell culture plates with complete DMEM including 10% FBS, until 100% of confluence. The monolayer was scratched and washed with PBS to remove non-adherent cells. Then, the cells were treated with Ru complexes for 24 hours. After this time, the monolayer was washed with PBS and stained with Giemsa. Digital images were taken using an Olympus BX51 inverted microscope with a digital camera. The inhibition of cell migration was analyzed with ImageJ software. The percentage (%) of migration was calculated using the following formula: 100-(final area/initial area × 100%).

Single cell lamellipodia formation

Cells were seeded on collagen and incubated in a humidified atmosphere with 10 % CO_2 in air at 37 °C for 24 h. After 24 h, digital images were taken using an Olympus BX51 inverted microscope with a digital camera from 10 fields; the cells with invaded extension were counted with imageJ.

DNA binding study

CT-DNA solutions of various concentrations dissolved in a saline solution (NaCl 0.09%) were added to the Ruthenium metal complexes 1 and 2. UV-visible absorption spectroscopy was recorded after equilibrium at room temperature for 10 min. The intrinsic binding constant Kb was determined by using Wolfe-Shimer equation.

$$\frac{[DNA]}{[\varepsilon a - \varepsilon f]} = \frac{[DNA]}{[\varepsilon b - \varepsilon f]} + \frac{[1]}{Kb[\varepsilon b - \varepsilon f]}$$

The absorption coefficients εa, εf, and εb correspond to Aobsd/ [complex], the extinction coefficient for the free complex and the extinction coefficient for the complex in the fully bound form, respectively. The intrinsic binding constant Kb can be obtained from the ratio of the slope to the intercept. It can be determined by monitoring the changes in the absorbance around of 260nm band at the corresponding absorbance DNA with increasing concentration of DNA and is given by the ratio of slope to the Y intercept in plots of [1/(ΔAbs) versus 1/[DNA]. For emission spectral, complex concentration was maintained constant as 10 μM and the concentration of DNA was varied from 0 to 250 μM. The emission enhancement factors were measured by comparing the intensities at 260nm under similar conditions [33].

Cytokinesis-block micronucleus assay

The cytokinesis-block micronucleus assay was set up with cultures in the logarithmic growth phase. Cells were seeded onto 6 well cell culture plates at a density of 50000 cells per well and were incubated at 37º C for 24 h. Then, the cells were treated with different concentrations of Ru compounds with Cytochalasin B (4.5 μg/mL) for 24 h. Bleomycin for 30 minutes used as positive control. Then, the cells were rinsed and subjected to hypotonic treatment with 0.075 % KCl at 37º C for 5 min, fixed with methanol at -20 C for 10 min, and stained with 5 % Giemsa solution. Cytochalasin B from Dreschslera dematioidea was purchased from Santa Cruz. Bleomycin (Blocamycin) was kindly provided by Gador (Buenos Aires, Argentina). For micronucleus assay, 1,000 binucleated cells were scored at x400 magnification per experimental point from each experiment. The examination criteria used were reported by Fenech [52].

Measurement of cell cycle/DNA content

The DNA content in G1/G0, S, and G2/M phases was analyzed using flow cytometry [53]. Cells were seeded in six-well plates and then treated with 2, 5, 5 and 10 μM Ru complexes for 24 h. The harvested cells were washed with PBS, fixed, and permeabilized with 70 % ice-cold ethanol for more than 2 h. Subsequently, the cells were resuspended in fresh staining buffer (15 mg/mL PI and 15 mg/mL DNase-free RNase prepared in PBS containing 2 mM EDTA) and incubated for 30 min at 37º C. Cell cycle distribution analysis was performed with a BD FACscalibur for data acquisition. For each sample,

View Article Online
DOI: 10.1039/C8MT00369F

cellular aggregates were gated out and at least 10,000 cells were counted and plotted on a single parameter histogram. The percentage of cells in the G1/G0, S, and G2/M phases and the sub-G1 peak was then calculated using FlowJo 7.6 (using the Watson model).

Apoptosis

Cells in early and late stages of apoptosis were detected with Annexin V-FITC and propidium iodide (PI) staining. Annexin V, fluorescein isothiocyanate (FITC), and propidium iodide (PI) were from Invitrogen (Buenos Aires, Argentina). Cells were treated with the three complexes and incubated for 24 h prior to analysis. For the staining, cells were washed with PBS and were diluted with 1X binding buffer. To 100 µL of cell suspension, 2.5 µL of Annexin V-FITC and 2 µL PI (250 µg/mL) were added and incubated for 15 min at room temperature prior to analysis. Cells were analyzed using flow cytometer (BD FACS Calibur™) and FlowJo 7.6 software. For each analysis 10,000 counts, gated on a FSC vs SSC dot plot, were recorded. Four subpopulations were defined in the dot plot: the undamaged vital (Annexin V−/PI−), the vital mechanically damaged (Annexin V/PI+), the apoptotic (Annexin V+/PI−), and the secondary necrotic (Annexin V+/PI+) subpopulations.

Multicellular spheroids formation

The development of multicellular spheroids was achieved by the hanging drop technique with minor modifications [54]. The cell suspension was adjusted to a concentration of 2400 cells/mL for MG-63 cell line, 2000 cells/ml for A549 cell line and 80000 cells/ml for MCF7 cell line. This concentration was selected to get 500 µm diameter spheroids at the beginning of the treatment with the compound. After 48 h, the compacted spheroids were transferred to an agar coated 96-well plate, and then, 200 µL of DMEM plus 10 % FBS were added to each well. The plate was cultured under the standard conditions for eight days, replacing 50 % of the culture media every 48 h for 1 week.

Treatment of multicellular spheroids with ruthenium complexes

For pharmacologic experiments, multicellular spheroids were treated in 96-well plates with 1 % DMSO in DMEM and with ruthenium complexes a range of concentration 50

to 500 µM in DMEM for 72 h. After that, cell viability of spheroids was achieved by the Resazurin reduction assay.

Invasion assays

This assay evidence the invasion potential of tumor cells [55]. The growth of multicellular spheroids was performed achieved by the hanging drop technique with minor modifications [54]. After that, the MCS were seeded on collagen solution (70 % collagen, 10% FBS, 10 % $NaHCO_3$, 10 % DMEM) and were incubated at 37 °C for 48 h. After that, the evaluation of cell invasion on collagen was achieved by image analysis (Image J).

Statistical analysis

Results are expressed as the mean of three independent experiments and plotted as mean ± standard error of the mean (SEM). The total number of repeats (*n*) is specified in the legends of the figures. Statistical differences were analyzed using the analysis of variance method followed by the test of least significant difference (Fisher). The statistical analyses were performed using STATGRAPHICS Centurion XVI.I.

Compliance with ethical standards

Conflict of interest: The authors declare that they have no conflict of interest.

Ethical approval: This article does not contain any studies with human participants or animals performed by any of the authors.

Funding: The work was supported by UNLP (11X/690), CONICET (PIP 0034), and ANPCyT (PICT 2014-2223, 2016-1574, 2016-0508 from Argentina and by the Slovenian Research Agency (P-0175).

Acknowledgments This work was partly supported by UNLP (11X/690), CONICET (PIP 0034), and ANPCyT (PICT 2014-2223, 2016-1574, 2016-0508 from Argentina and by the Slovenian Research Agency (P-0175). IEL and ALDV are members of the Carrera

View Article Online
DOI: 10.1039/C8MT00369F

del Investigador, CONICET, Argentina. MCR has a fellowship from ANPCyT, Argentina.

References

1 L. A. Torre, F. Bray, R. L. Siegel, J. Ferlay, J. Lortet-Tieulent and A. Jemal, *CA. Cancer J. Clin.*, 2015, **65**, 87–108.

2 M. O. Palumbo, P. Kavan, W. H. Miller, L. Panasci, S. Assouline, N. Johnson, V. Cohen, F. Patenaude, M. Pollak, R. T. Jagoe and G. Batist, *Front. Pharmacol.*, 2013, **4**, 57.

3 U. Ndagi, N. Mhlongo and M. Soliman, *Drug Des. Devel. Ther.*, 2017, **Volume11**, 599–616.

4 I. E. León, J. F. Cadavid-Vargas, A. L. Di Virgilio and S. Etcheverry, *Curr. Med. Chem.*

5 T. C. Johnstone, K. Suntharalingam and S. J. Lippard, *Chem. Rev.*, 2016, **116**, 3436–86.

6 I. Kostova, *Curr. Med. Chem.*, 2006, **13**, 1085–107.

7 E. Alessio and L. Messori, in *Metallo-Drugs: Development and Action of Anticancer Agents*, eds. A. Sigel, H. Sigel, E. Freisinger and R. K. O. Sigel, De Gruyter, Berlin, Boston, 2018, vol. 18.

8 S. Thota, D. A. Rodrigues, D. C. Crans and E. J. Barreiro, *J. Med. Chem.*, 2018, acs.jmedchem.7b01689.

9 R. Trondl, P. Heffeter, C. R. Kowol, M. a. Jakupec, W. Berger and B. K. Keppler, *Chem. Sci.*, 2014, **5**, 2925–2932.

10 A. Bergamo and G. Sava, *Chem. Soc. Rev.*, 2015, **44**, 8818–35.

11 M. Abid, F. Shamsi and A. Azam, *Mini Rev. Med. Chem.*, 2016, **16**, 772–86.

12 S. H. Liang, A. G. Southon, B. H. Fraser, A. M. Krause-Heuer, B. Zhang, T. M. Shoup, R. Lewis, I. Volitakis, Y. Han, I. Greguric, A. I. Bush and N. Vasdev, *ACS Med. Chem. Lett.*, 2015, **6**, 1025–9.

13 V. Prachayasittikul, S. Prachayasittikul, S. Ruchirawat and V. Prachayasittikul, *Drug Des. Devel. Ther.*, 2013, **7**, 1157–78.

14 O. Afzal, S. Kumar, M. R. Haider, M. R. Ali, R. Kumar, M. Jaggi and S. Bawa, *Eur. J. Med. Chem.*, 2015, **97**, 871–910.

15 W.-Q. Ding and S. E. Lind, *IUBMB Life*, 2009, **61**, 1013–8.

16 C. Martín Santos, S. Cabrera, C. Ríos-Luci, J. M. Padrón, I. López Solera, A. G. Quiroga, M. a Medrano, C. Navarro-Ranninger and J. Alemán, *Dalton Trans.*, 2013, **42**, 13343–8.

17 M. Gobec, J. Kljun, I. Sosič, I. Mlinarič-Raščan, M. Uršič, S. Gobec and I. Turel, *Dalton Trans.*, 2014, **43**, 9045–51.

18 I. E. León, P. Díez, E. J. Baran, S. B. Etcheverry and M. Fuentes, *Metallomics*, 2017, **9**, 891–901.

19 A. Mitrović, J. Kljun, I. Sosič, S. Gobec, I. Turel and J. Kos, *Dalton Trans.*, 2016, **45**, 16913–16921.

20 M. J. Pushie, K. H. Nienaber, K. L. Summers, J. J. H. Cotelesage, O. Ponomarenko, H. K. Nichol, I. J. Pickering and G. N. George, *J. Inorg. Biochem.*, 2014, **133**, 50–6.

21 K. S. O. Ferraz, D. C. Reis, J. G. Da Silva, E. M. Souza-Fagundes, E. J. Baran and H. Beraldo, *Polyhedron*, 2013, **63**, 28–35.

22 J. Kljun, I. E. León, Š. Peršič, J. F. Cadavid-Vargas, S. B. Etcheverry, W. He, Y. Bai and I. Turel, *J. Inorg. Biochem.*, 2018, **186**, 187–196.

23 M. D. Živković, J. Kljun, T. Ilic-Tomic, A. Pavic, A. Veselinović, D. D. Manojlović, J. Nikodinovic-Runic and I. Turel, *Inorg. Chem. Front.*, 2018, **5**, 39–53.

24 M. Gobec, J. Kljun, I. Sosič, I. Mlinarič-Raščan, M. Uršič, S. Gobec and I. Turel, *Dalton Trans.*, 2014, **43**, 9045–51.

25 M. Kubanik, H. Holtkamp, T. Söhnel, S. M. F. Jamieson and C. G. Hartinger, *Organometallics*, 2015, **34**, 5658–5668.

26 T. Mosmann, *J. Immunol. Methods*, 1983, **65**, 55–63.

27 R. Trondl, P. Heffeter, C. R. Kowol, M. A. Jakupec, W. Berger and B. K. Keppler, *Chem. Sci.*, 2014, **5**, 2925–2932.

28 F. Ciccarese and V. Ciminale, *Front. Oncol.*, 2017, **7**, 117.

29 S. M. Meier-Menches, C. Gerner, W. Berger, C. G. Hartinger and B. K. Keppler, *Chem. Soc. Rev.*, 2018, **47**, 909–928.

30 M. S. de Camargo, R. A. De Grandis, M. M. da Silva, P. B. da Silva, M. M. Santoni, C. E. Eismann, A. A. Menegário, M. R. Cominetti, C. F. Zanelli, F. R. Pavan and A. A. Batista, *BioMetals*, , DOI:10.1007/s10534-018-0160-0.

31 M. Tian, J. Li, S. Zhang, L. Guo, X. He, D. Kong, H. Zhang and Z. Liu, *Chem. Commun.*, 2017, **53**, 12810–12813.

32 K. Nakamoto, M. Tsuboi and G. D. Strahan, *Drug-DNA interactions : structures and spectra*, John Wiley & Sons, 2008.

33 A. I. Matesanz, E. Jimenez-Faraco, M. C. Ruiz, L. M. Balsa, C. Navarro-Ranninger, I. E. León and A. G. Quiroga, *Inorg. Chem. Front.*, 2018, **5**, 73–83.

34 H. Stopper and S. O. Müller, *Toxicol. In Vitro*, 1997, **11**, 661–7.

35 Z. Adhireksan, G. E. Davey, P. Campomanes, M. Groessl, C. M. Clavel, H. Yu, A. A. Nazarov, C. H. F. Yeo, W. H. Ang, P. Dröge, U. Rothlisberger, P. J. Dyson and C. A. Davey, *Nat. Commun.*, 2014, **5**, 3462.

36 X. Chen, F. Gao, W.-Y. Yang, Z.-X. Zhou, J.-Q. Lin and L.-N. Ji, *Chem. Biodivers.*, 2013, **10**, 367–384.

37 A. Srishailam, N. M. Gabra, Y. P. Kumar, K. L. Reddy, C. S. Devi, D. Anil Kumar, S. S. Singh and S. Satyanarayana, *J. Photochem. Photobiol. B Biol.*, 2014, **141**, 47–58.

38 M. S. de Camargo, M. M. da Silva, R. S. Correa, S. D. Vieira, S. Castelli, I. D'Anessa, R. De Grandis, E. Varanda, V. M. Deflon, A. Desideri and A. A. Batista, *Metallomics*, 2016, **8**, 179–192.

39 F. Mello-Andrade, C. G. Cardoso, C. R. E. Silva, L. Chen-Chen, P. R. de Melo-Reis, A. P. de Lima, R. Oliveira, I. B. M. Ferraz, C. K. Grisolia, M. A. P. Almeida, A. A. Batista and E. de P. Silveira-Lacerda, *Biomed. Pharmacother.*, 2018, **107**, 1082–1092.

40 M. Hassan, H. Watari, A. AbuAlmaaty, Y. Ohba and N. Sakuragi, *Biomed Res. Int.*, 2014, **2014**, 1–23.

41 J. Chen, Y. Zhang, G. Li, F. Peng, X. Jie, J. She, G. Dongye, Z. Zou, S. Rong and L. Chen, *J. Biol. Inorg. Chem.*, 2018, **23**, 261–275.

42 B. Xu, Z. Sun, Z. Liu, H. Guo, Q. Liu, H. Jiang, Y. Zou, Y. Gong, J. A. Tischfield and C. Shao, *PLoS One*, 2011, **6**, e18618.

43 A. Mazouzi, G. Velimezi and J. I. Loizou, *Exp. Cell Res.*, 2014, **329**, 85–93.

44 J. L. Chen, T. W. J. Steele and D. C. Stuckey, *Environ. Sci. Technol.*, 2015, **49**, 13463–13471.

45 E. Schreiber-Brynzak, E. Klapproth, C. Unger, I. Lichtscheidl-Schultz, S. Göschl, S. Schweighofer, R. Trondl, H. Dolznig, M. A. Jakupec and B. K. Keppler, *Invest. New Drugs*, 2015, **33**, 835–47.

46 K. B. Desoize B, Collery P, Akéli JC, *Met Ions Biol Med*, 2000, **6**, 6:573–576.

47 J. Carlsson and T. Nederman, *Eur. J. Cancer Clin. Oncol.*, 1989, **25**, 1127–33.

48 L. A. Hazlehurst and W. S. Dalton, *Cancer Metastasis Rev.*, 2001, **20**, 43–50.

49 J. T. Erler, C. J. Cawthorne, K. J. Williams, M. Koritzinsky, B. G. Wouters, C. Wilson, C. Miller, C. Demonacos, I. J. Stratford and C. Dive, *Mol. Cell. Biol.*, 2004, **24**, 2875–89.

50 S. Göschl, E. Schreiber-Brynzak, V. Pichler, K. Cseh, P. Heffeter, U. Jungwirth, M. A. Jakupec, W. Berger and B. K. Keppler, *Metallomics*, 2017, **9**, 309–322.

51 G. Rainaldi, A. Calcabrini, G. Arancia and M. T. Santini, *Anticancer Res.*, **19**, 1769–78.

52 M. Fenech, *Mutat. Res.*, 2000, **455**, 81–95.

53 I. E. Leon, V. Porro, A. L. Di Virgilio, L. G. Naso, P. A. M. Williams, M. Bollati-Fogolín and S. B. Etcheverry, *J. Biol. Inorg. Chem.*, 2014, **19**, 59–74.

54 I. E. León, J. F. Cadavid-Vargas, A. Resasco, F. Maschi, M. A. Ayala, C. Carbone and S. B. Etcheverry, *JBIC J. Biol. Inorg. Chem.*, 2016, **21**, 1009–1020.

55 E. B. Berens, J. M. Holy, A. T. Riegel and A. Wellstein, *J. Vis. Exp.*, , DOI:10.3791/53409.

View Article Online
DOI: 10.1039/C8MT00369F

Table 1 IC_{50} and SI values of complex 1 and 2 in several cell lines after 24 h.

	IC_{50} (**1**)	SI (**1**)	IC_{50} (**2**)	SI (**2**)	IC_{50} (CDDP)	SI(CDDP)
MG-63	19.7 ± 0.6	2.21	12.2 ± 1.4	2.26	39 ± 1.8	0.29
A549	50.9 ± 5.3	0.85	24.9 ± 6.5	1.10	114 ± 2.3	0.10
MCF7	45.1 ±3.1	0.96	20.5 ± 1.5	1.35	42 ± 3.2	0.23
MDA-MB-231	31.7 ± 2.3	1.37	15.4 ± 0.3	1.79	131 ±18	0.085
L929	43.5 ± 8.5		27.6 ± 3.7		11.2 ± 1.6	

Table 2. Percentage of early and late apoptotic events on MG-63, A549 and MCF7 cells.

MG-63	Annexin V+/ PI -	Annexin V+/ PI +	Annexin V-/ PI +
Control	1.0 ± 0.3	0.8 ± 0.2	5.1 ± 0.6
1 (5 μM)	2.3 ± 0.7	2.0 ± 0.6	6.8 ± 2.4
1 (10 μM)	1.5 ± 0.2	2.1 ± 0.5	10.4 ± 2.6
2 (5 μM)	0.9 ± 0.3	0.6 ± 0.1	9.7 ±2.8
2 (10 μM)	3.7 ± 1.1	2.2 ± 0.8	4.7 ± 1.2
A549			
Control	1.9 ±0.3	0.5 ± 0.1	1.98 ±0.7
1 (5 μM)	2.5 ± 0.7	0.4 ± 0.2	5.1 ± 0.6
1 (10 μM)	0.7 ± 0.2	0.4 ± 0.1	3.7 ± 0.4
2 (5 μM)	2.1 ± 0.3	0.3 ± 0.03	2.5 ± 0.8
2 (10 μM)	1.6 ± 1.2	0.2 ± 0.01	3.6 ± 0.3
MCF7			
Control	0.43 ± 0.02	2.3 ± 0.3	6.7 ± 0.4
1 (5 μM)	1.4 ± 0.2	7.0 ± 0.9	5.1 ± 0.5
1 (10 μM)	1.0 ± 0.2	16.1 ± 2.7	9.8 ± 0.9
2 (5 μM)	2.1 ± 0.8	17.3 ± 1.5	10.2 ± 3.0
2 (10 μM)	1.0 ± 0.4	27.1 ± 0.4	37.8 ± 2.0

View Article Online
DOI: 10.1039/C8MT00369F

Table 3. IC_{50} values of complex **1**, **2** and CDDP in multicellular spheroids of MG-63, A549 and MCF-7.

	IC_{50} (**1**)	IC_{50} (**2**)	CDDP
MG-63	251.2 ± 14.7	360.9 ± 7.9	65.1 ± 5.6
A549	103.9 ± 10.8	213.6 ± 8.6	>500
MCF7	158.3 ± 5.8	364.2 ± 6.3	129.5 ± 9.3

View Article Online
DOI: 10.1039/C8MT00369F

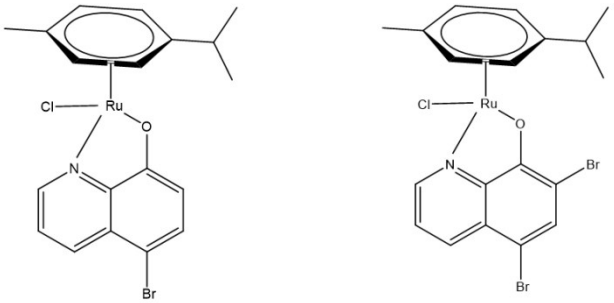

Figure 1. Structures proposed for Ru complexes 1 and 2 [22].

338x190mm (96 x 96 DPI)

View Article Online
DOI: 10.1039/C8MT00369F

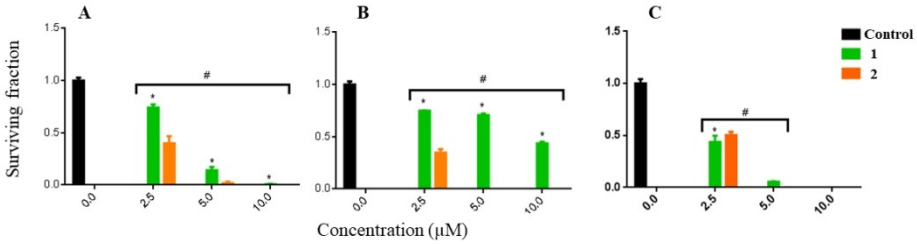

Figure 2. Clonogenic assay. Effect of complex 1 and 2 on MG-63 (A), A549 (B) and MCF-7 (C) cell lines viability. Cells were incubated in Dulbecco's modified Eagle's medium (DMEM) alone (control) or with different concentrations (2.5, 5 and 10 μM) of compounds 1 and 2. The results are expressed as surviving fraction as the percentage of the basal level and represent the mean ± the standard error of the mean (SEM) (n = 18). # $p<0.05$ differences between control and treatment, *$p<0.05$ differences between treatment of complex 1 and complex 2.

338x190mm (96 x 96 DPI)

View Article Online
DOI: 10.1039/C8MT00369F

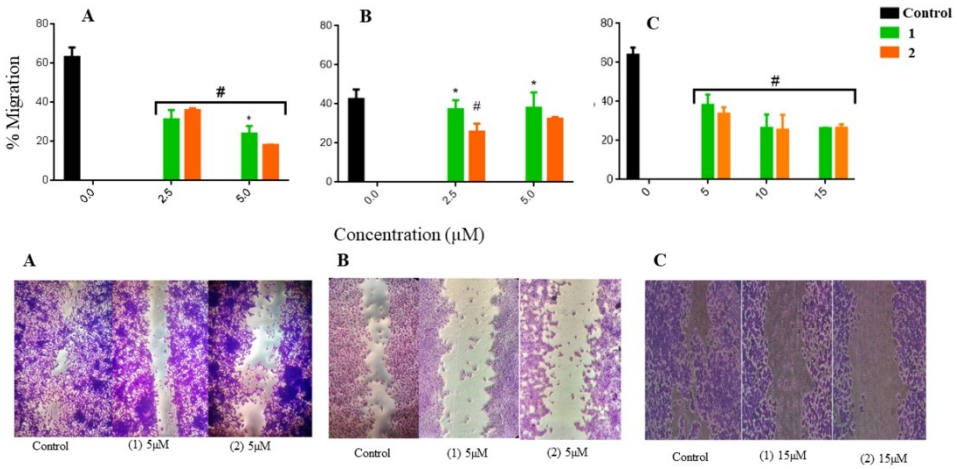

Figure 3. Wound healing assay. (A) MG-63, (B) A549 and (C) MCF7 # p< 0.05 differences between control and treatment with compounds. * p<0.05 differences between treatment of complex 1 and complex 2.

338x190mm (96 x 96 DPI)

View Article Online
DOI: 10.1039/C8MT00369F

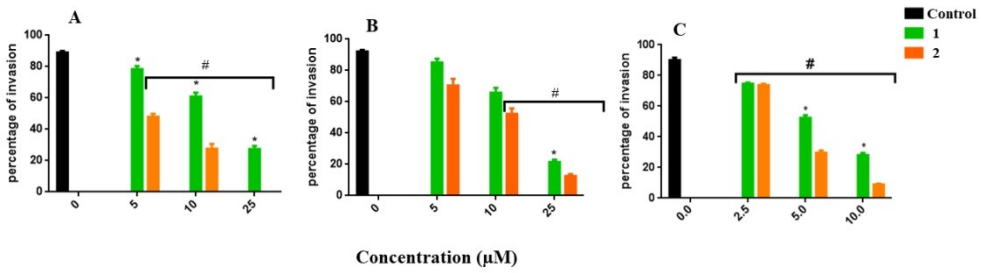

Figure 4. Invasion assay. Effect of complex 1 and 2 on MG-63 (A), A549 (B) and MCF7 (C) single cell lamellipodia formation. # $p<0.05$ differences between control and treatment, *$p<0.05$ differences between treatment of complex 1 and complex 2.

338x190mm (96 x 96 DPI)

View Article Online
DOI: 10.1039/C8MT00369F

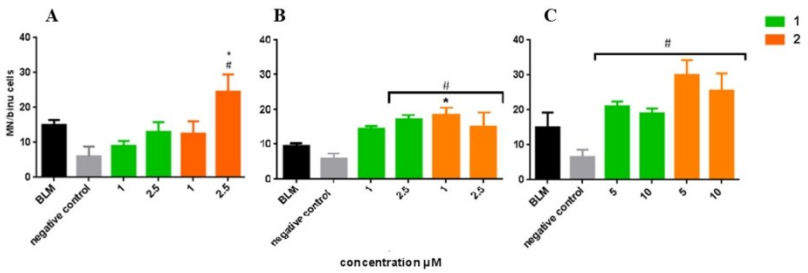

Figure 5. Micronucleus assay. Genotoxicity of complex 1 and 2 toward MG-63 (A) A549 (B) and MCF-7 (C) tumor cells. # p<0.001 differences between control and treatment, *p<0.001 differences between treatment of complex 1 and complex 2. BLM: bleomycin (positive control).

338x190mm (96 x 96 DPI)

View Article Online
DOI: 10.1039/C8MT00369F

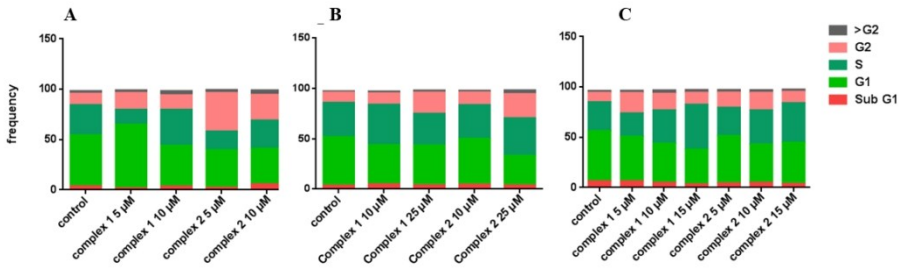

Figure 6. Effect of complex 1 and 2 on cell cycle arrest and DNA fragmentation on MG-63 (A), A549 (B) and MCF-7 (C) cells.

338x190mm (96 x 96 DPI)

View Article Online
DOI: 10.1039/C8MT00369F

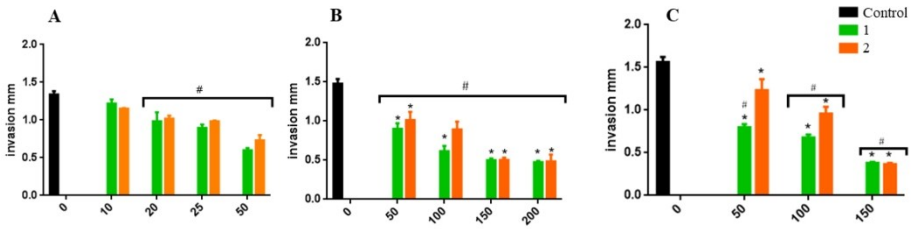

Figure 7. Effect of complex 1 and 2 on migration of 3D spheroids on MG-63 (A), A549 (B) and MCF-7 (C) cells. # $p<0.05$ differences between control and treatment, *$p<0.05$ differences between treatment of complex 1 and complex 2.

338x190mm (96 x 96 DPI)